

Frame selection techniques for the Magellan adaptive optics VisAO camera.

Jared R. Males, Laird M. Close, Derek Kopon, Victor Gasho, Katherine Follette
Steward Observatory, University of Arizona, USA

ABSTRACT

The Magellan AO system will begin commissioning in early 2012. Its VisAO camera will provide 20 mas FWHM images with mean Strehl ratios of ~ 0.2 in R band on a 6.5m telescope. Depending on seeing conditions, Strehl ratio may reach temporary peaks as high as 0.5 at these wavelengths. To take advantage of these brief periods of high performance, we plan to adopt lucky imaging style data taking and reduction techniques. As part of this effort we have developed a novel real-time frame selection technique, which will use AO system telemetry and a fast shutter to limit CCD exposure to these very brief moments of higher Strehl. Here we describe the expected benefits of our frame selection techniques in various operating modes. We also present the results of laboratory characterization of the shutter, and describe the performance of predictive algorithms used to control it.

Keywords: adaptive optics, visible adaptive optics, lucky imaging, frame selection, simulations

1. INTRODUCTION

The Magellan adaptive optics (AO) system will install a near clone of the Large Binocular Telescope (LBT) Adaptive Secondary Mirrors (ASM) at the 6.5m Magellan Clay telescope at Las Campanas Observatory (LCO), Chile. The high performance of the LBT ASM has recently been demonstrated on sky using one of the two 8.4m primary mirrors on Mt. Graham, Az. When deployed with the smaller Magellan primary, the relatively higher projected actuator pitch will provide good performance at shorter wavelengths. This has motivated the development of a visible wavelength AO system, which we call VisAO. The Magellan AO system is described extensively elsewhere in these proceedings, including an overview,¹ a description of the optical design and lab tests of the innovative atmospheric dispersion corrector (ADC),² and our planned integral field spectrograph (IFS).³ The design of the ADC was presented previously.⁴

The Magellan (and LBT) AO systems use ASMs, a technology proven at the MMT telescope on Mt. Hopkins, Az.⁵ By minimizing the number of warm surfaces in the optical train, the thermal performance of the system is improved. An important innovation being used by the LBT is the pyramid wavefront sensor (WFS). A significant improvement this provides over a conventional Shack-Hartmann WFS is the ability to re-bin the detector, which improves its performance on faint guide stars. To take advantage of these capabilities BLINC/MIRAC4 will be used for $10\mu\text{m}$ imaging,⁶ grism spectroscopy,⁷ and nulling interferometry.⁸

For VisAO, we make use of the already installed e2v CCD47 with Scimeasure Little Joe controller, which is used as an acquisition camera at LBT. This 1024x1024 camera provides 0.0085" pixels, Nyquist sampling the diffraction limited PSF down to $0.55\mu\text{m}$ with an 8.7" field of view (FOV). A key feature of this design regarding VisAO performance is that the CCD47 is on a common mount with the WFS. With the exception of 2 reflections,² most tip-tilt will be sensed and removed by the WFS with minimal non-common vibrations between it and our science camera. Figure 1 illustrates the design of our Magellan AO WFS and VisAO optical board.

Some residual tip-tilt will still be present at the science focal plane. In addition, working at short visible wavelengths with such a small PSF core ($\sim 20\text{mas}$) means that even a few mas of non-common vibrations (from, say, the WFS beamsplitter) will significantly degrade our long exposure PSF. This fact has motivated the design of an additional tip-tilt control loop, based on the Andor LUCA electron multiplying CCD (EMCCD). This device will primarily use light reflected from a near-focus "coronagraphic" occulting dot (made of chrome) to

Further author information: (Send correspondence to J.R.M.)
J.R.M.: E-mail: jrmales@as.arizona.edu

Adaptive Optics Systems II, edited by Brent L. Ellerbroek, Michael Hart, Norbert Hubin, Peter L. Wizinowich,
Proc. of SPIE Vol. 7736, 773660 · © 2010 SPIE · CCC code: 0277-786X/10/\$18 · doi: 10.1117/12.858055

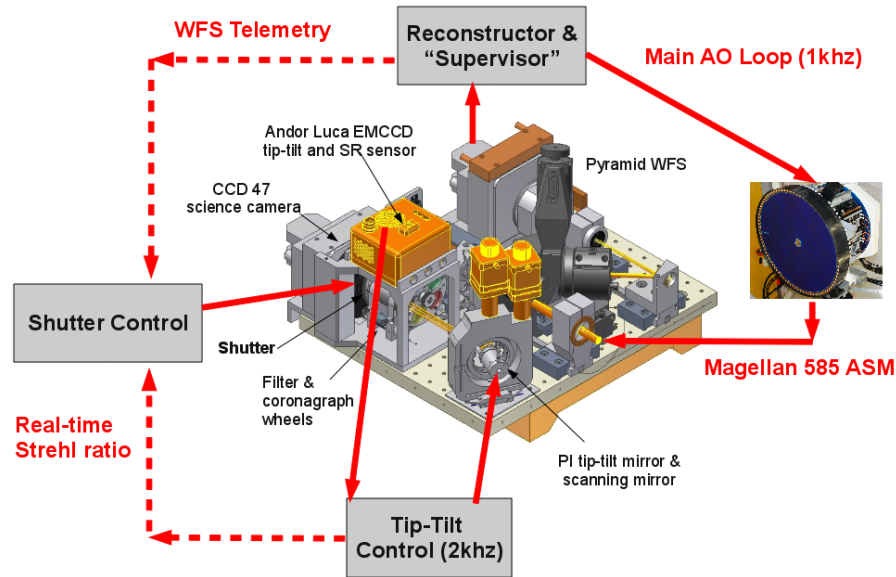


Figure 1. The Magellan AO system WFS and VisAO camera. The main AO loop (typically controlled at 1 kHz), the VisAO specific tip-tilt loop (which can operate at 2 kHz) and the path of telemetry used to control the shutter are shown schematically.

sense tip-tilt and instantaneous Strehl ratio. The tip-tilt signal will control a fast independent tip-tilt mirror. The Strehl signal will be used to control a fast shutter in a novel lucky-imaging-like technique we describe in this paper. For a full description of our tip-tilt control design, see Close et al.¹ and Kopon et al.² in these proceedings.

Lucky imaging is a technique which selects the best images from a series of short exposures, then shifts and adds them to produce a final image with higher resolution than a single long exposure. First proposed by Fried⁹ to counter the effects of atmospheric seeing, it is now in common use at several telescopes.¹⁰ It has also been adapted for use with an AO system, where the correction quality in the visible is typically low, but has short peaks of high Strehl.^{11, 12} By selecting based on Strehl ratio, it has been shown that both resolution¹¹ (measured by full width at half maximum (FWHM)) and sensitivity¹³ (measured by signal-to-noise ratio (S/N)) can be improved.

To be effective, lucky imaging typically uses very short exposures, requiring cameras that operate faster than ~ 10 frames-per-second (fps). For normal astronomical CCDs this imposes a significant readout noise (RON) penalty, as each read will produce a few electrons of noise which then quickly adds to overwhelm faint signals. This has been overcome to great effect using EMCCDs, which offer very low RON - typically $\sim 0.1e^-$ per read¹⁴ - when operated in the photon counting mode. Photon counting EMCCDs have some (small) drawbacks though. If flux is higher than 1 photon/pixel/read the device effectively has its quantum efficiency (QE) lowered by 50%.¹⁵ In our visible AO system we will always have a very bright guide star in our FOV, and with only low to moderate Strehl ratios we will have a bright uncorrected halo from the star spread over the detector, making this QE penalty impossible to ignore.

An additional issue we identified with any lucky imaging system is the trade-off between FOV and camera speed. The isoplanatic patch at visible wavelengths at LCO will typically be $\sim 4''$ in radius. To provide good sampling across this FOV we need a 1024x1024 array. When we began the investigations detailed here the fastest EMCCD cameras of this size could only be operated at ~ 10 fps (EMCCDs have since become a little faster, now achieving ~ 30 fps over arrays of this size). As we will show 10 fps isn't quite fast enough to fully take advantage of the peaks in Strehl ratio, which are typically shorter than 100ms in our simulations. The common solution with an EMCCD is to window such a device and operate at 50fps or faster, which also helps to mitigate

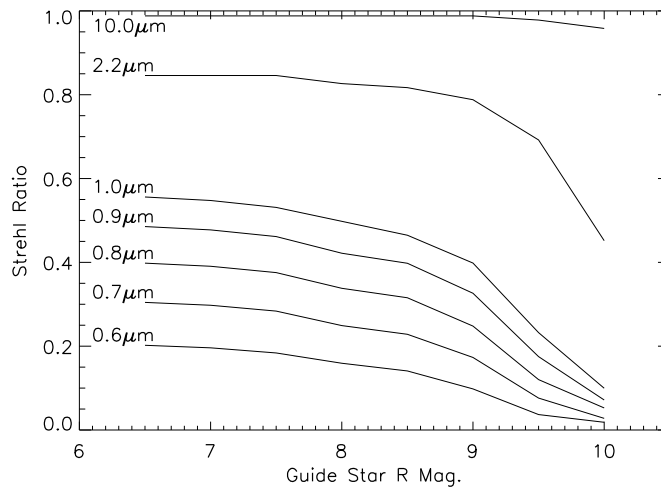


Figure 2. Simulated performance of the Magellan AO system vs. guide star R magnitude for 75th percentile seeing at LCO. Based on CAOS simulations as described in the text, each curve includes the error terms listed Table 1. Though there is not currently a K band camera planned for this system, we provide a 2.2 μm curve to allow comparison with other systems. BLINC/MIRAC4 will provide 10 μm imaging and nulling interferometry, and as shown by these results performance in N band is expected to be very good. Since the primary focus of this paper is performance at visible wavelengths, we do not present results for fainter guide stars where VisAO will not perform well. We expect VisAO to consistently provide Strehl ratios > 0.2 for bright guide stars, and usable correction out to at least $R=9.5$.

the high-flux penalty. This carries its own drawback in that FOV is cut by 25%, which for many observations is itself equivalent to a QE penalty.

A final consideration, and perhaps most important, is that the Magellan VisAO system is largely based on already designed instruments, both in the case of our main imager (the CCD47) and our plans for a visible wavelength IFS.³ Since the CCD47 is used as an acquisition camera integral to AO system operation, changing detectors was judged too risky to overall performance. Our IFS plans are based on using a pre-existing spectrograph with relatively simple modifications for accepting fibers from the VisAO system. Changing detectors would significantly increase the cost of this system, but we still desire to take advantage of frame selection.

Given the bright guide star specific and FOV vs. speed drawbacks of EMCCD based lucky imaging, and the pre-existing system designs, we have developed a new imaging concept which we call real time frame selection (RTFS). In this mode of operation, we will make use of a high speed mechanical shutter and telemetry from the AO system to only expose our CCD47 when Strehl is high. The shutter is both fast and responsive enough to provide the equivalent temporal resolution of a 100fps camera, and can do this over the entire 8.7" FOV of our 1024x1024 array. As we will show, this technique can improve resolution (when compared with doing nothing) by nearly 100% of λ/D .

In this paper we first describe our simulations of the Magellan AO system. We use these simulations to predict performance vs. guide star magnitude at various wavelengths, and we have also used the output to develop and test the RTFS technique. We then present a model of S/N in AO imaging, which we use to analyze the costs and benefits of frame selection and to compare different imaging techniques. Using this model and the output of our simulations we calculate the performance of an ideal RTFS system both in terms of resolution and sensitivity. Finally, we describe our current progress in implementing RTFS. We have procured and tested a mechanical shutter which meets the demanding requirement of RTFS. An area of ongoing development is Strehl prediction, necessary because of a short but unavoidable delay in shutter actuation time.

VisAO 0.7 μ m Error Budget for an R=7 G2 Guide Star			
Error Term	Est. (nm)	Sim. (nm)	notes
Fitting	77.2	...	Estimates from standard thumb-rules. ²⁰ These are added in quadrature for loop total.
Servo	47.4	...	
Recon.	47.0	...	
Loop Total	102.1	102.4	CAOS simulations as described in the text.
Static.	30	30	Based on LBT design specifications.
Non-Com. Path	30	30	Based on VisAO design specifications.
Resid. T/T	52.6	52.6	For 5 mas residual. ²¹
Total	122.4	122.7	Sum in quadrature.
0.7 μ m Strehl	0.3	0.3	Using extended Marechal approximation.

Table 1. The VisAO error budget for a spectral type G2 R=7 magnitude guide star. Assumptions include $r_0 = 14\text{cm}$ at 550nm, science wavelength of 0.7 μm , and the LCO site atmosphere layer model. Estimates using standard AO thumb-rules agree very well with our simulation results. For this analysis the assumed performance of our VisAO tip-tilt loop is 5mas r.m.s. At 10mas r.m.s. tip-tilt control our long exposure Strehl would degrade to 0.2.

2. PERFORMANCE SIMULATIONS OF THE MAGELLAN AO SYSTEM

To assess the performance of the Magellan AO system we have been making use of the Code for Adaptive Optics System (CAOS) package.¹⁶ This IDL based “problem solving environment” provides good off-the-shelf functionality and flexibility, and has been used to simulate the LBT AO system.¹⁷

Our atmosphere model is derived from the GMT site survey of LCO.¹⁸ We use 6 turbulent layers with C_n^2 and wind speed and direction as determined by the survey. We also made use of recent work establishing $L_0 = 25\text{m}$ at LCO.¹⁹ Based on these data we use von Karman turbulence with $r_0 = 14\text{cm}$ as our performance baseline, which corresponds to the $\sim 75^{\text{th}}$ percentile at LCO.¹⁸

The CAOS calibration procedure allows us to calculate interaction matrices for various pyramid sensor configurations. A typical simulation for a bright (R ~ 7 mag) guide star uses 392 modes with 1 khz sampling, a gain of 0.4, pyramid modulation of $2\lambda/D$, and pyramid sensor CCD39 parameters based on the manufacturer specification. We simulate with 1ms time steps and apply a 2ms delay to each update to account for WFS readout, calculations, and mirror motion. For each setup (guide star magnitude, etc.) we allow 100ms for loop closing, and then run the simulation for 2 seconds of loop time. At each time step we save a simulated science image at various wavelengths. These images are stored with no sources of noise and we use a 1nm wide bandpass, which allows us to make a very accurate Strehl measurement. The Strehl ratio at each point is measured by comparison to a perfect Airy pattern for a 6.5m telescope with a 0.29 central obscuration. We typically use the mean short exposure Strehl from these time series, since this value does not include tip-tilt (which we add in quadrature from our error budget).

Table 1 shows the error budget for the Magellan AO system in R band on a spectral type G2 R=7 magnitude guide star. We compare estimates for the fitting, servo, and reconstruction errors with our CAOS simulation results and find good agreement. The error calculated from simulations is based on the mean short exposure Strehl ratio. We then add (in quadrature) the unsimulated errors from static mirror aberrations, non-common path aberrations, and finally the long exposure degradation of Strehl due to tip-tilt. In Figure 2 we show our simulation-based performance predictions vs. guide star magnitude at various wavelengths. These curves are calculated in similar fashion to the Strehl in Table 1, with appropriate differences for wavelength.

3. THE COSTS & BENEFITS OF FRAME SELECTION

In this paper we introduce our RTFS technique, and describe the results of our initial attempts to implement it on simulated data. To assess the benefits of frame selection, we use a simple model of the AO imaging process to calculate S/N and the output of our CAOS simulations to determine the resulting resolution. The following development relies heavily on the work of Racine et al.,²² and benefits from the work of Law et al.^{10–12} and Gladysz et al.^{13, 23, 24}

3.1 A Generic Frame Selection Algorithm

Before we can analyze its benefits, we first state what we mean by frame selection. To do this we will develop a general description of a selection algorithm, leaving specific details for later.

We begin by collecting a stream of raw data at a time t_i , such as AO control loop telemetry or short exposure science image pixels, with n elements

$$\vec{X}(t_i) = \begin{bmatrix} x_1(t_i) \\ \vdots \\ x_n(t_i) \end{bmatrix}.$$

Next the data is converted to a set of m attributes[‡] by some operation F

$$\vec{Y}(t_i) = \begin{bmatrix} y_1(t_i) \\ \vdots \\ y_m(t_i) \end{bmatrix} = F(\vec{X}(t_i)).$$

For instance, F may include the calculation of slopes given the raw WFS pixels or sub-aperture counts. Finally we use a classifier G to determine whether some image quality metric, say Strehl ratio S , is above some threshold value, say S_T . The classifier uses the previous l samples of the m attributes, possibly with a delay of k time steps (meaning the classifier is also a predictor):

$$G(\vec{Y}(t_i), \dots, \vec{Y}(t_{i-l+1})) = \begin{cases} 0 & \text{if } S(t_{i+k}) < S_T \\ 1 & \text{if } S(t_{i+k}) \geq S_T. \end{cases} \quad (1)$$

The value of G represents the decision whether to include the data at t_{i+k} in the final image. We explicitly allow for prediction since this will be necessary for the real time implementation we discuss later. Finally we note that this formulation does not require that the actual value of the image quality metric (e.g. S) be calculated. This opens the door to using, for instance, machine learning classification techniques without *a priori* knowledge of relationships between the raw data and image quality.

The standard lucky imaging technique can be described using this algorithm. In this case, the data vector $\vec{X}(t_i)$ is made up of the pixel values of a short exposure image at time t_i . The corresponding attribute is just the Strehl Ratio $S(t_i)$, and the operation F is the reduction pipeline which results in the Strehl ratio measurement. The classifier G is a simple comparison between the measured $S(t_i)$ and S_T . In standard Lucky imaging only the current time step is used and no prediction is performed, i.e. $k = 0$ and $l = 1$.

Another implementation of this algorithm is RTFS (discussed above), under development for the Magellan VisAO system, which is used to control a camera shutter in real time. The primary goal of this technique is to minimize the number of detector reads, while gaining the benefits of frame selection. We will discuss our algorithm further in Section 3.3.

3.2 Signal to Noise Ratio and Duty Cycle

The obvious drawback to frame selection is that only a fraction of the telescope time allotted to the observation is used in the final result. This fraction can be thought of as the duty cycle \mathcal{DC} . The act of throwing away the fraction $(1 - \mathcal{DC})$ of the signal can be expected to negatively effect the sensitivity of the observation. It might be true, however, that by keeping only the “good” frames we can overcome this loss in signal by reducing the noise in our final image, and this has been demonstrated on-sky.¹³ In conventional lucky imaging, one always has all the data available from an observation and so has lost no telescope time. In RTFS, however, we will irretrievably lose the time when the shutter is closed and so we must understand the trade-offs with sensitivity for this technique.

To that end, we use a simple model of the S/N in AO imaging, based heavily on that developed by Racine et al.²² with only slight modifications, to determine the net efficiency cost of frame selection. Here we skip most of

[‡]It is not necessary that $m = n$

the derivation and present the results for the limiting cases most likely to be encountered in natural guide star (NGS) AO. A full derivation using our notation will be presented in a forthcoming paper.

Our S/N model is

$$S/N = \frac{\mathcal{E} f_c \sqrt{DCt}}{(\mathcal{E} f_c + \bar{S} \bar{\mathcal{P}}(\theta) f_* n + (1 - \bar{S}) H(\theta) f_* n + 0.53 \tau_0 [(1 - \bar{S}) H(\theta) f_* n]^2 + N_{sky} n + N_{det} n)^{\frac{1}{2}}}, \quad (2)$$

where f_* and f_c are the flux (photons sec^{-1}) at the telescope of the central star and the companion (located at separation θ); \mathcal{E} is the total flux enclosed in the photometric aperture; DC is the duty cycle (discussed above); $\bar{\mathcal{P}}$ is the point spread function (PSF), ideally an obscured Airy pattern, averaged by tip-tilt; n is the number of pixels contained in the photometric aperture; $H(\theta)$ is the uncorrected halo flux per pixel; τ_0 is the speckle lifetime;²² N_{sky} is the per-pixel flux due to sky background (BG); and N_{det} is the per-pixel flux due to detector noise. The quantity \bar{S} is the mean short exposure Strehl, which we use rather than the long exposure (tip-tilt degraded) Strehl ratio to account for the guide star's halo contribution to the noise as it is what quantifies the relative fraction of flux in the halo. Using the long exposure Strehl here would make the halo noise too large.

3.2.1 Encircled Energy and Aperture Size

The fraction of incident photons contained in a circular aperture assuming a perfect obscured-Airy PSF is given by²⁵

$$\mathcal{E}_{\mathcal{P}}(\rho) = \frac{1}{1 - \epsilon^2} \left((1 + \epsilon^2)(1 - J_0^2(\rho) - J_1^2(\rho)) - 4\epsilon \int_0^\rho \frac{J_1(t) J_1(\epsilon t)}{t} dt \right) \quad (3)$$

where ϵ is the telescope central obscuration and ρ is the aperture size. Now in an AO corrected image only a fraction \bar{S} of the flux is contained in the diffraction limited component of the PSF, and $(1 - \bar{S})$ is contained in the halo. Following Racine et al.²² we adopt the function

$$H(\theta) = \frac{0.488}{W_h^2} \left[1 + \frac{11}{6} \left(\frac{\theta}{W_h} \right)^2 \right]^{-11/6}. \quad (4)$$

to describe the uncorrected halo, where W_h is a width parameter.

We can integrate equation (4) to calculate the fraction of the incident photons in the halo encircled by an aperture of size ρ :

$$\mathcal{E}_H(\rho) = 1 - \left(1 + \frac{11}{6} \left(\frac{\rho}{W_h} \right)^2 \right)^{-5/6}. \quad (5)$$

Racine et al.²² argued that the halo contribution to flux could safely be ignored since its S/N would be comparatively low. While this is likely true for the high Strehls now routinely achieved in the infrared, in the visible we expect only low to moderate Strehls. At Magellan, with $\epsilon = 0.29$, the enclosed fraction is $\mathcal{E}_{\mathcal{P}} = 0.747$ for $\rho = 1.12\lambda/D$ (the first Airy minimum). From simulations we derive a value of $W_h = 0.23''$ at $\lambda = 0.7\mu\text{m}$, so $\mathcal{E}_H = 0.018$. For $S = 0.1$ then

$$\frac{(1 - S)\mathcal{E}_H}{S\mathcal{E}_{\mathcal{P}} + (1 - S)\mathcal{E}_H} = 0.18$$

is a non-negligible fraction of the total signal collected by the photometric aperture defined by the first Airy minimum. This means that we must account for the halo component of the PSF of the science object and so can't assume that \mathcal{E} is simply proportional to S .

In our simulations we have found that the usual model just employed of a diffraction limited core on top of a partially corrected halo has limited ability to describe the location of the photons in our image. At low Strehls, imperfect correction causes the core to broaden, and the PSF tends to elongate in the direction of the prevailing winds. Even at higher Strehls residual telescope jitter can have the same effect. We also consider it desirable to avoid relying on an analytic model for the PSF, especially the halo component as this is likely to depend

greatly on atmospheric seeing and guide star brightness. In practice, we find that using elliptical apertures fit to contours of constant flux will give consistent results from our simulated data.

Now let $\mathcal{A} = \mathcal{E}/n$ be the average fractional photon flux per pixel in the ellipse described by $\vec{x} = (a, b, \phi)$, which are the semi-major axis, semi-minor axis, and orientation of the ellipse. If we then define \vec{x}^* as the aperture which maximizes S/N, then the optimum faint companion detection S/N is

$$S/N = \frac{\mathcal{A}(\vec{x}^*)f_c\sqrt{\mathcal{DC}tn^*}}{(\mathcal{A}(\vec{x}^*)f_c + \bar{S}\bar{\mathcal{P}}(\theta; \epsilon)f_* + (1 - \bar{S})H(\theta)f_* + 0.53\tau_0[(1 - \bar{S})H(\theta)f_*]^2n^* + N_{sky} + N_{det})^{\frac{1}{2}}}. \quad (6)$$

where $n^* = \pi a^*b^*$. We have gone to this effort because we find that using other algorithms to estimate S/N, such as peak-pixel or a fixed aperture size, tends to incorrectly analyze the benefits of frame selection in our simulations in various cases - especially when the contribution of the companion's halo component is ignored.

3.2.2 Effective Duty Cycle

Now we can solve Equation (6) for the time t it takes to reach a desired S/N:

$$t = \frac{(S/N)^2}{\mathcal{A}^2(\vec{x}^*)n^*f_c^2\mathcal{DC}} (\mathcal{A}(\vec{x}^*)f_c + \bar{S}\bar{\mathcal{P}}(\theta; \epsilon)f_* + (1 - \bar{S})H(\theta)f_* + 0.53\tau_0[(1 - \bar{S})H(\theta)f_*]^2n^* + N_{sky} + N_{det}).$$

We can then compare two data taking techniques, e.g. frame selection to simple integration. In order for a technique to provide a S/N advantage then the effective duty cycle $\mathcal{DC}_{\text{eff}}$ must satisfy the inequality

$$\mathcal{DC}_{\text{eff}} = \frac{t_o}{t_1} \geq 1 \quad (7)$$

where t_o is the the time needed to reach a S/N goal with simple integration (i.e. doing nothing), and t_1 is the time needed with a particular frame selection technique.

The effective duty cycle concept allows us to compare the trade-offs between resolution, encircled energy, and efficiency, and then decide the optimal imaging technique for our AO system and science goals. Now we consider the limiting cases of equations (6) and (7) which we expect to routinely encounter with Magellan AO. By choosing cases where specific sources of noise dominate we can compare imaging techniques without specifying details such as companion brightness and separation, or the desired S/N.

3.2.3 The Speckle Limited Case

Several differential imaging techniques are in common use to reduce the impact of the coherent speckle noise in high contrast imaging (cf. ADI, SDI, ASDI²⁶). These techniques each have weaknesses, typically being less effective close to the guide star and when used on extended objects such as a circumstellar disk. SDI also requires a strong spectral feature in the companion when compared to the guide star. In cases where speckle suppression cannot be achieved and the term $0.53\tau_0[(1 - \bar{S})H(\theta)f_*]^2n^*$ dominates in Equation (6), then Equation (7) reduces to

$$\mathcal{DC}_{eff}^{sp} = \mathcal{DC}_1 \left(\frac{\mathcal{A}_1^*}{1 - \bar{S}_1} \right)^2 \left(\frac{1 - \bar{S}_o}{\mathcal{A}_o^*} \right)^2. \quad (8)$$

It is apparent from this expression that if, through frame selection, we can increase \bar{S}_1 and/or \mathcal{A}_1^* we will have at least some compensation for the loss of efficiency represented by $\mathcal{DC}_1 < 1$. Furthermore, given the right conditions, frame selection has the potential to maintain or even improve sensitivity while delivering the higher resolution represented by increased \bar{S} and \mathcal{A}_1^* .

3.2.4 The Halo Limited Case

If we are able to suppress the speckles, then when the term $(1 - \bar{S})H(\theta)f_*$ dominates in equation (6) we are in the halo photon-noise limited regime. Equation (7) then becomes

$$\mathcal{DC}_{eff}^h = \mathcal{DC}_1 \left(\frac{(\mathcal{A}_1^*)^2 n_1^*}{1 - \bar{S}_1} \right) \left(\frac{1 - \bar{S}_o}{(\mathcal{A}_o^*)^2 n_o^*} \right) \quad (9)$$

Once again we see that if we can increase \bar{S}_1 and/or \mathcal{A}_1^* we have some leeway with lower \mathcal{DC}_1 . It should also be noted that the S/N maximizing aperture will be different between this case and the speckle limited case above due to the different dependence on n^* .

3.2.5 Background and Read Noise Limited

The next limiting case that should be considered occurs when the dominate noise terms are due to sky BG and detector RON. However, the present work is focused on bright NGS AO. In this regime, we will almost always be limited by halo noise (photon and speckle) within the FOV of our camera. As such, we will only state here, without proof, that because RTFS allows arbitrarily long integrations the detector read-noise performance can be competitive with the current generation of EMCCDs. When we also consider that RTFS allows us to do this over our entire detector FOV without windowing, RTFS retains its competitiveness even for wider separations from faint stars.

3.3 Simulated Faint Guide Star Strehl Selection

Now that we have a framework for comparing imaging techniques, we investigate the performance of an ideal RTFS technique on an observation simulated with CAOS. The setup of this simulation was nearly identical to that described in Section 2, except seeing was set to the median $r_0 = 18cm$. For an R=10 mag A5V guide star the loop is stable, but undergoes significant fluctuation in correction quality. We ran the simulation with this guide star for 5 seconds of observation time, and extracted the simulated image at the CCD47 at 1 ms intervals and measured Strehl on each of these short frames. We then applied the same corrections for static and non-common-path aberrations to the 1ms measurements as in Table 1, but do not use the tip-tilt correction on the 1ms frames.

Next, we establish a threshold S_T and stack each 1ms frame which is above this value. On the combined frame, we then fit elliptical contours at various flux levels. For the reasons described in Section 3.2.1 we use these contours as apertures to calculate the enclosed flux and number of pixels, and then choose the S/N maximizing aperture for the speckle and halo limited cases. Finally we measure the FWHM resolution using the 50% peak flux contour. The results of this algorithm for various thresholds are shown in Figure 3.

The very competitive design choice for our system would be to use an EMCCD as the science camera. To study the trade-offs with RTFS, we assume a 1024x1024 array which can be operated at 10fps with negligible read noise. We also assume a QE penalty of 50% when flux is greater than 1 electron/pixel/read. The same simulated frames used for RTFS are combined in 100ms exposures, and we then apply the typical Lucky imaging method of shifting these longer frames before adding based on S_T . In Figure 4 we compare this technique to RTFS. When flux is low, EMCCD based lucky provides a large \mathcal{DC}_{eff} advantage due to the resolution boost from shift-and-add, however the ultimate resolution achieved is $\sim 10\%$ worse due to the lower temporal resolution. For brighter objects, or those close to a bright guide star, the EMCCD based lucky performs worse due to the QE reduction.

An important caveat to this discussion is that we have assumed that the EMCCD “QE reduction”, which is actually due to an increase in photon noise, applies identically to the speckle noise in the speckle limited case. This is almost certainly not strictly true, but rather depends on subtle details such as the plate scale and speckle lifetime. As such, the lower lucky-imaging curves in Figure 4 should be considered merely an illustration of the point, and actual performance in this case could be better or worse.

A further consideration is the impact of our S/N maximizing apertures. In the speckle-limited case this is almost always the peak pixel due to the strong dependence on the number of pixels in the aperture. Photometry is seldom conducted on a single pixel, however, and so the performance of frame selection (whether real-time or

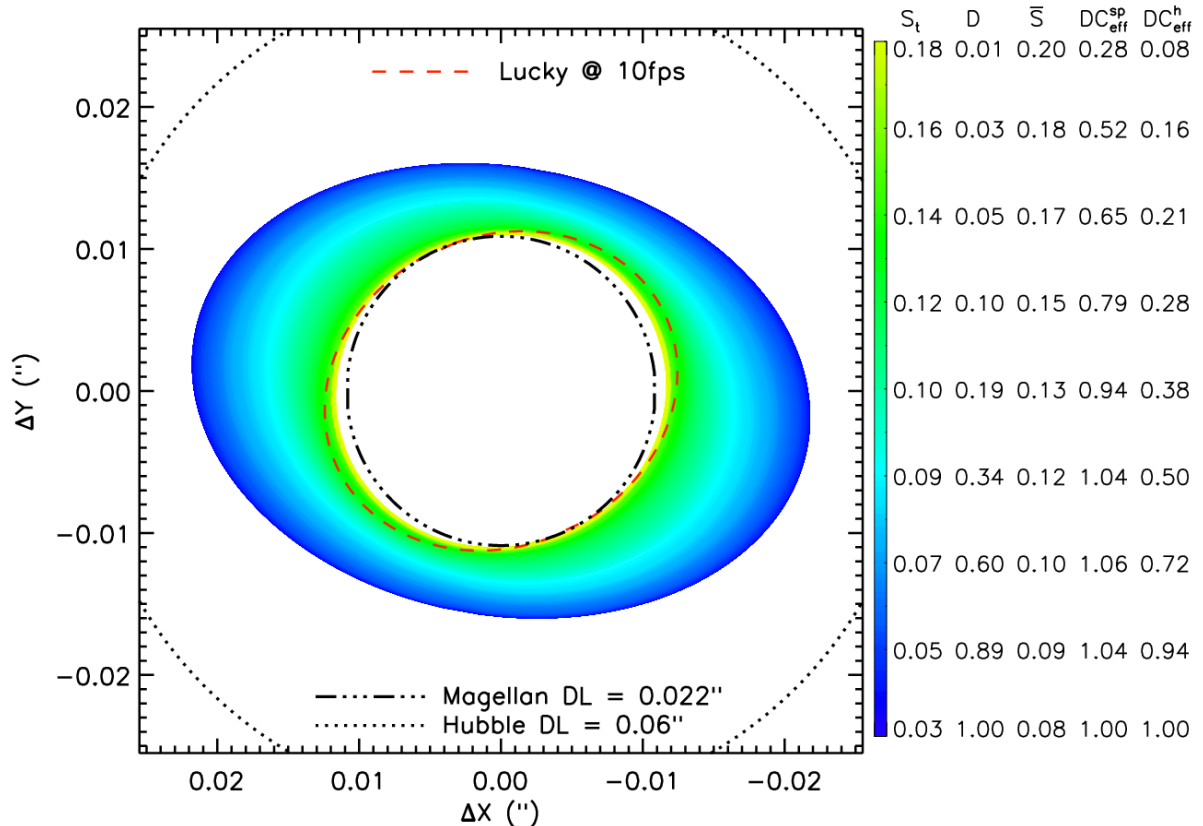


Figure 3. Results from Strehl selection on an $R=10$ guide star, showing FWHM contours corresponding to various selection thresholds. The colorbar encodes the threshold S_t and resultant gross duty cycle \mathcal{DC} for each contour, as well as the resultant mean Strehl \bar{S} and \mathcal{DC}_{eff} for the speckle and halo limited cases. We see that significant gains in resolution can be achieved, and compare these gains to those possible with 10 fps lucky imaging. For comparison the diffraction limits (DL) of the Magellan VisAO system and the Hubble Space Telescope (HST) are plotted.

conventional lucky) is understated here if one uses a larger aperture. This is somewhat true in the halo limited case as well, as the optimum aperture tends to be $< 1\lambda/D$ in radius, which is probably also smaller than normally used.

Finally we assume a tip-tilt loop with ~ 5 mas rms control, simulated by shifting the 1ms images before applying the RTFS algorithm (we did not simulate the dynamic performance of our tip-tilt loop). The correction of residual atmospheric tip-tilt (~ 15 mas rms) provides a huge improvement in \mathcal{DC}_{eff} . Interestingly, the achievable resolution is the same without tip-tilt control. This is because at very high thresholds, only a small fraction of the simulated data is used. This implies that by accepting only the best images, the dominant source of resolution degradation (Strehl loss) is rejected and residual tip-tilt has a smaller effect.

The main conclusion of this effort is that RTFS has potential to provide significant gains in resolution and sensitivity - with some trade-offs between the two - similar to conventional Lucky imaging. The benefit of RTFS is that these can be realized over the full FOV of a camera, and with its full QE, using already installed detectors. With our newly designed VisAO tip-tilt loop, the gains from RTFS have potential to be quite dramatic: we could more than double our VisAO observing efficiency while nearly attaining diffraction limited resolution.

4. RTFS IMPLEMENTATION

Having established that RTFS offers significant performance enhancement for the Magellan VisAO system, our next step is to develop algorithms to provide real-time control of our fast shutter and to test the performance

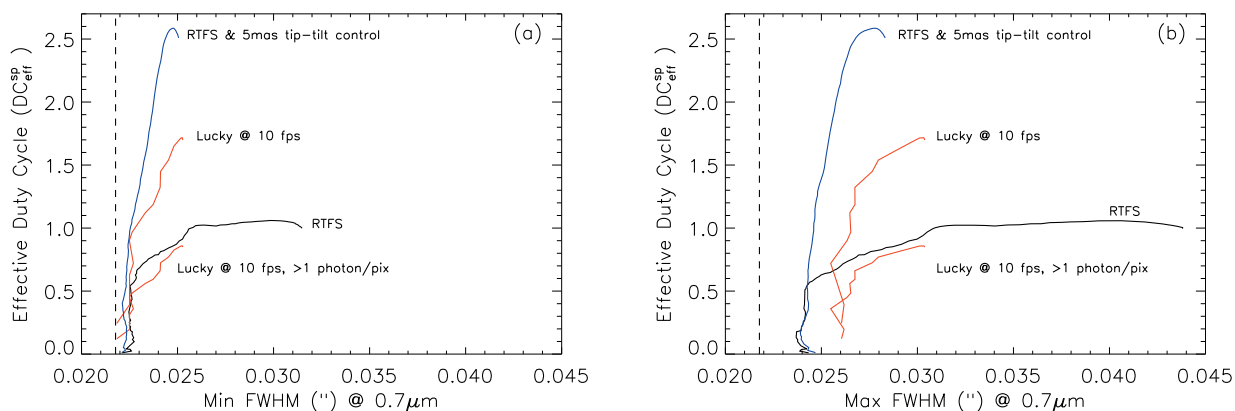


Figure 4. Results from Strehl selection on an $R=10$ guide star, showing the effective duty cycle vs the resultant resolution for the speckle limited case. Minimum FWHM (a) corresponds to the semi-minor axis of the elliptical contours shown in Figure 3, and maximum FWHM (b) likewise to the semi-major axis. We compare the results with those possible with a 10 fps EMCCD (which has a 50% QE penalty for bright targets). We also show the significant improvement possible with the combination of a fast tip-tilt loop and RTFS - this system could potentially more than double observing efficiency in the speckle limited case.

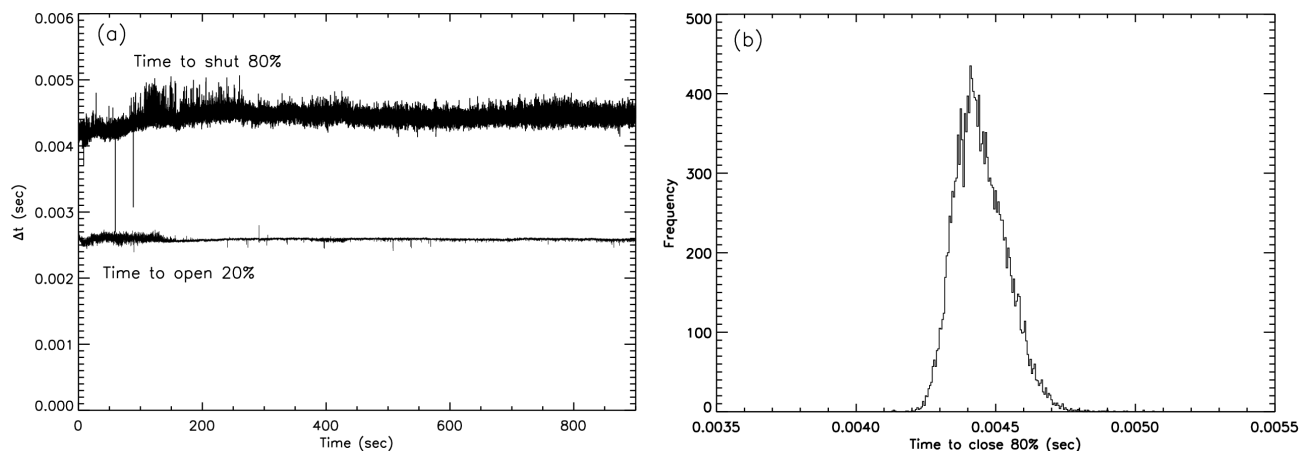


Figure 5. Performance of the VS-25 shutter. In (a) we present the time to open and shut while the VS-25 shutter was operated at 25hz continuously (50 fps equivalent, with $\mathcal{DC} = 50\%$). As proxies for full open and shut we use the time to change an LED-photosensor circuit, which corresponds to 80% open and 20% shut. After a few minutes of warm up time the device is very stable. We show the histogram of the 80% shut times after 200 s has elapsed in (b). The standard deviation of this distribution is $\sigma = 92.5\mu\text{s}$, and the open distribution has $\sigma = 11.2\mu\text{s}$. For 180,000 cycles, a total exposure of 1 hour, the uncertainty in exposure time will be 55ms, or 0.002%.

limitations of available shutters.

4.1 Mechanical Shutter Performance

The Magellan VisAO project has chosen the Uniblitz VS-25 mechanical shutter to begin prototyping our RTFS system. This shutter has a 25mm aperture, and is capable of operation at up to 40hz. Here we follow the manufacturer and discuss shutter speed in terms of a complete open and shut cycle, so 40hz implies 12.5ms exposures if we use a symmetric square wave pulse. This is equivalent to 80 fps with $\mathcal{DC} = 0.5$, over the full FOV of our 1024x1024 detector. The minimum exposure time of the shutter is $\sim 10\text{ms}$, and it can be operated asynchronously. This gives us the time-resolution equivalent to a 100 fps camera.

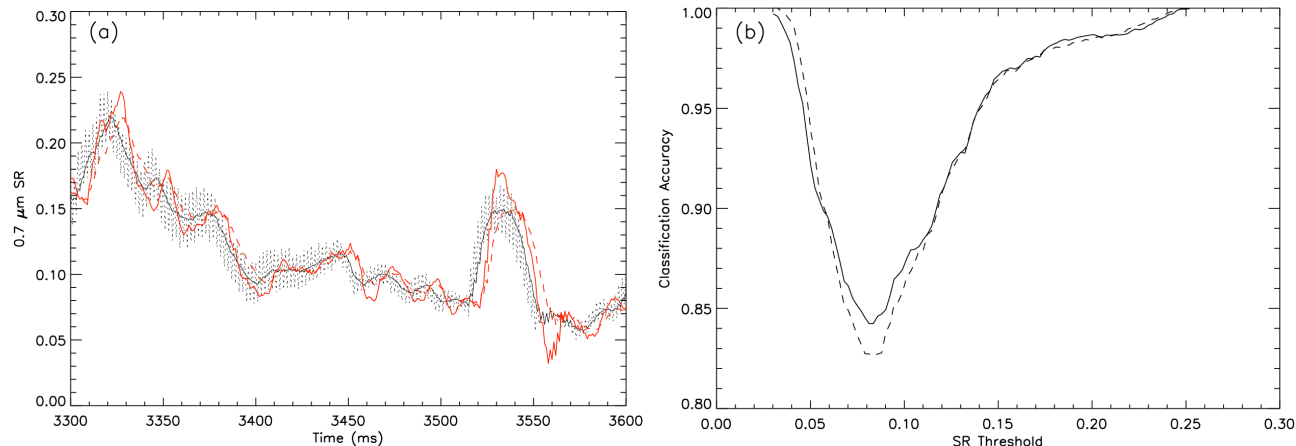


Figure 6. Strehl predictions. In part (a) we show a raw time series from the simulation described in Section 3.3, zoomed into a representative section. The solid black line is the output of the FIR digital filter designed to have a minimal phase lag. The dashed red line is the “prediction” result of applying the current filtered Strehl measurement with a 6ms shutter actuation delay. The solid red line is the prediction output of using an average of two different linear extrapolations. In (b) we present the classification accuracy of these two prediction strategies vs. Strehl selection threshold.

We have performed a series of bench tests to determine the accuracy and stability of the VS-25. Our device has an LED-photosensor synchronization circuit, which is interrupted by one of the two shutter blades. The state change of this circuit occurs at 80% shut and 20% open. Figure 5 shows the results of one of these tests at 25hz, which is equivalent to 50 fps. We have found the timing of the shutter motion to be very reliable and stable. If we operated the shutter at 25hz for 2 hours, to obtain a total exposure of 1 hour, the resulting uncertainty in exposure time would only be 55ms, or 0.002%.

4.2 Strehl Classification Algorithms

We can place the RTFS problem in the formalism established in section 3.1. In the simplest case, where we are using the high speed output of our tip-tilt sensor, the data vector $\vec{X}(t_i)$ consists of Strehl measurements, or simply the value of the brightest pixel. To start we can simply use these measurements as input to the classifier G , with a delay of k time steps set by the mechanical performance of our shutter. The main problem with this approach is that we suffer errors due to the delay. We also must deal with noise in a real system, and desire to reject moments of classification change which are shorter than our shutter actuation times (e.g. a 1ms long dip barely below the threshold should not close the shutter). To counter these we have been investigating real-time digital filters and various prediction algorithms.

We have previously investigated the use of wavefront sensor (WFS) telemetry exclusively to estimate Strehl ratio.²⁷ Due to the advent of our fast tip-tilt control loop design we have more recently been concentrating on using its output to directly estimate and predict Strehl. In future work we will investigate the benefits of combining WFS telemetry with the direct measurements. For now, however, we report only on our most recent results using direct Strehl measurements.

As discussed, it is necessary to condition the Strehl time series. The tip-tilt loop will typically be operated at very high frame rates (1-3 khz), faster than the main AO loop. Simulations indicate that this produces a sawtooth pattern in the signal, with sharp increases when the latest correction is applied followed by decreases between corrections. At such short exposure times photon noise may become important on fainter stars as well. Due to the mechanical limitations of a shutter (i.e. minimum cycle time and finite response times) we must filter out these high frequency components of the signal. Since this system will operate in real time, this filter must be causal and must have a minimum phase lag. To accomplish this we used the Matlab digital filter design tool (fdatool) to determine coefficients for a finite impulse response (FIR) filter. This ninth order low-pass FIR filter has a pass frequency of 50 hz and a stop frequency of 75 hz, and was optimized for a minimum phase lag. In terms of the generic selection algorithm, this filter serves as the operator F and the filtered-signal output

becomes the input to the classifier G . Figure 6 illustrates the performance of this filter on a simulated Strehl time series.

To accomplish prediction, we have found good performance with simple linear extrapolation. Our experiments with various fitting intervals indicate that combining the results of various intervals can improve performance, especially near peaks and valleys in the signal. By interval we mean the number of previous data points used for fitting. Based on the manufacturer specifications for the shutter to be used, we extrapolate 6ms in the future. Figure 6 compares the prediction results of averaging 4 step and 10 step fitting intervals with no prediction.

Figure 6 also shows the classification accuracy of these two approaches. From Equation (1) we know that this is a binary problem, which makes it significantly easier to analyze compared to attempting to calculate the exact value of Strehl ratio. In the right hand panel of Figure 6 it is apparent that with a real time source of Strehl measurements we can achieve very good classification accuracy. The simple algorithms we are considering here struggle a little at lower thresholds (0.05 – 0.10). Considering Figure 3, where we find that our best resolution is achieved at thresholds $S_t > \sim 0.15$, these simple techniques appear quite sufficient as accuracy is $> 95\%$.

5. CONCLUSION

We expect the Magellan VisAO system to provide some of the highest resolution filled aperture astronomical images ever obtained when it is commissioned in early 2012. Our simulations indicate that we will have low to moderate Strehl ratios for wavelengths less than $1.0\mu\text{m}$. As is typical for such observations, we will see large fluctuations in correction quality over short periods of time. To compensate for this we plan to utilize a novel frame selection technique, which will provide the ability to reliably achieve the diffraction limit while offering sensitivity and efficiency improvements.

To understand the costs and potential benefits of frame selection, which unavoidably involves discarding valuable telescope time, we have employed a simple model of S/N in AO imaging. Using this model we have developed a simple framework to compare various imaging strategies, and shown that our new RTFS technique is very competitive when compared to short-exposure based lucky imaging. This is especially true in NGS visible AO where the presence of a bright star in our FOV makes the use of low-RON EMCCDs challenging.

We have demonstrated that commercially available mechanical shutters provide the timing accuracy and precision to support RTFS. It was also shown that with a real time source of short exposure Strehl ratio measurements we can obtain very accurate frame selection. The combination of a fast VisAO specific tip-tilt loop and RTFS should more than double our observing efficiency and consistently provide diffraction limited images at the 6.5m Magellan Clay telescope.

REFERENCES

- [1] Close, L. M., Gasho, V., Kopon, D., Males, J. R., Follette, K., Brutlag, K., Uomoto, A., and Hare, T., “The Magellan Telescope Adaptive Secondary AO System: AO Science in the Visible and Mid-IR,” *Proc. SPIE* **7736**, (2010).
- [2] Kopon, D., Close, L. M., Males, J. R., Gasho, V., and Follette, K., “The Magellan adaptive secondary VisAO Camera: diffraction-limited broadband visible imaging and 20mas fiber array IFU,” *Proc. SPIE* **7736**, (2010).
- [3] Follette, K., Close, L. M., Kopon, D., Males, J. R., and Gasho, V., “The first VisAO-fed integral field spectrograph: MagAO IFS,” *Proc. SPIE* **7735**, (2010).
- [4] Kopon, D., Close, L. M., and Gasho, V., “An advanced atmospheric dispersion corrector for extreme AO,” *Proc. SPIE* **7015**, (2008).
- [5] Wildi, F. P., Brusa, G., Lloyd-Hart, M., Close, L. M., and Riccardi, A., “First light of the 6.5-m MMT adaptive optics system,” *Proc. SPIE* **5169**, 17–25 (2003).
- [6] Skemer, A. J., Close, L. M., Hinz, P. M., Hoffmann, W. F., Kenworthy, M. A., and Miller, D. L., “Evidence for Misaligned Disks in the T Tauri Triple System: 10 μm Superresolution with MMTAO and Markov Chains,” *APJ* **676**, 1082–1087 (2008).

- [7] Skemer, A. J., Close, L. M., Hinz, P. M., Hoffmann, W. F., Greene, T. P., Males, J. R., and Beck, T. L., “ISM Dust Grains and N-band Spectral Variability in the Spatially Resolved Subarcsecond Binary UY Aur,” *APJ* **711**, 1280–1290 (2010).
- [8] Hinz, P. M., Angel, J. R. P., Woolf, N. J., Hoffmann, W. F., and McCarthy, D. W., “BLINC: a testbed for nulling interferometry in the thermal infrared,” *Proc. SPIE* **4006**, 349–353 (2000).
- [9] Fried, D. L., “Probability of getting a lucky short-exposure image through turbulence,” *JOSA* **68**, 1651–1657 (1978).
- [10] Law, N. M., Mackay, C. D., and Baldwin, J. E., “Lucky imaging: high angular resolution imaging in the visible from the ground,” *A&A* **446**, 739–745 (2006).
- [11] Law, N. M., Mackay, C. D., Dekany, R. G., Ireland, M., Lloyd, J. P., Moore, A. M., Robertson, J. G., Tuthill, P., and Woodruff, H. C., “Getting Lucky with Adaptive Optics: Fast Adaptive Optics Image Selection in the Visible with a Large Telescope,” *APJ* **692**, 924–930 (2009).
- [12] Law, N. M., Dekany, R. G., Mackay, C. D., Moore, A. M., Britton, M. C., and Velur, V., “Getting lucky with adaptive optics: diffraction-limited resolution in the visible with current AO systems on large and small telescopes,” *Proc. SPIE* **7015**, (2008).
- [13] Gladysz, S., Christou, J., Law, N., Dekany, R., Redfern, M., and Mackay, C., “Lucky imaging and speckle discrimination for the detection of faint companions with adaptive optics,” *Proc. SPIE* **7015**, (2008).
- [14] Daigle, O., Carignan, C., Gach, J., Guillaume, C., Lessard, S., Fortin, C., and Blais-Ouellette, S., “Extreme Faint Flux Imaging with an EMCCD,” *PASP* **121**, 866–884 (2009).
- [15] Mackay, C., Basden, A., and Bridgeland, M., “Astronomical imaging with L3CCDs: detector performance and high-speed controller design,” *Proc. SPIE* **5499**, 203–209 (2004).
- [16] Carbillet, M., Vérinaud, C., Femenía, B., Riccardi, A., and Fini, L., “Modelling astronomical adaptive optics - I. The software package CAOS,” *MNRAS* **356**, 1263–1275 (2005).
- [17] Carbillet, M., Vérinaud, C., Esposito, S., Riccardi, A., Puglisi, A., Femenía, B., and Fini, L., “Performance of the first-light adaptive optics system of LBT by means of CAOS simulations,” *Proc. SPIE* **4839**, 131–139 (2003).
- [18] Thomas-Osip, J. E., Prieto, G., Johns, M., and Phillips, M. M., “Giant Magellan Telescope site evaluation and characterization at Las Campanas Observatory,” *Proc. SPIE* **7012**, (2008).
- [19] Floyd, D. J. E., Thomas-Osip, J., and Prieto, G., “Seeing, Wind, and Outer Scale Effects on Image Quality at the Magellan Telescopes,” *PASP* **122**, 731–742 (2010).
- [20] Roddier, F., “Adaptive Optics in Astronomy,” ch. 2: Imaging through the atmosphere, 9, Cambridge University Press (1999).
- [21] Sandler, D. G., Stahl, S., Angel, J. R. P., Lloyd-Hart, M., and McCarthy, D., “Adaptive optics for diffraction-limited infrared imaging with 8-m telescopes,” *JOSAA* **11**, 925–945 (1994).
- [22] Racine, R., Walker, G. A. H., Nadeau, D., Doyon, R., and Marois, C., “Speckle Noise and the Detection of Faint Companions,” *PASP* **111**, 587–594 (1999).
- [23] Gladysz, S., Christou, J. C., Bradford, L. W., and Roberts, L. C., “Temporal Variability and Statistics of the Strehl Ratio in Adaptive-Optics Images,” *PASP* **120**, 1132–1143 (2008).
- [24] Gladysz, S., Christou, J. C., and Redfern, M., “Characterization of the Lick adaptive optics point spread function,” *Proc. SPIE* **6272**, (2006).
- [25] Mahajan, V. N., “Uniform versus Gaussian beams: a comparison of the effects of diffraction, obscuration, and aberrations,” *JOSAA* **3**(4), 470–485 (1986).
- [26] Oppenheimer, B. R. and Hinkley, S., “High-Contrast Observations in Optical and Infrared Astronomy,” *ARAA* **47**, 253–289 (2009).
- [27] Kopon, D., Males, J., Close, L. M., and Gasho, V., “Enabling technologies for visible adaptive optics: the Magellan adaptive secondary VisAO camera,” *Proc. SPIE* **7439**, (2009).